

Divalent metal ion-based catalytic mechanism of the Nudix hydrolase Orf153 (YmfB) from *Escherichia coli*

Myoung-Ki Hong,^{a,†}
António J. M. Ribeiro,^{b,†}
Jin-Kwang Kim,^{a,†}
Ho-Phuong-Thuy Ngo,^a Jiyoung
Kim,^c Choong Hwan Lee,^c
Yeh-Jin Ahn,^d Pedro Alexandrino
Fernandes,^b Qing Li,^e Maria Joao
Ramos^{b,*} and Lin-Woo Kang^{a,e,*}

^aDepartment of Biological Sciences, Konkuk University, 1 Hwayang dong, Gwangjin-gu, Seoul 143-701, Republic of Korea, ^bRequimte/ Departamento de Química e Bioquímica, Faculdade de Ciências, Universidade do Porto, Rua do Campo Alegre s/n, 4169-007 Porto, Portugal, ^cDepartment of Bioscience and Biotechnology and Bio/Molecular Informatics Center, Konkuk University, 1 Hwayang dong, Gwangjin-gu, Seoul 143-701, Republic of Korea, ^dDepartment of Green Life Science, College of Convergence, Sangmyung University, 7 Hongji-dong, Jongno-gu, Seoul 110-743, Republic of Korea, and ^eSchool of Pharmaceutical Sciences, Center for Cellular and Structural Biology, Sun Yat-sen University, Guangzhou 510006, People's Republic of China

† These authors contributed equally to this paper.

Correspondence e-mail: mjrmos@fc.up.pt, lkang@konkuk.ac.kr

YmfB from *Escherichia coli* is the Nudix hydrolase involved in the metabolism of thiamine pyrophosphate, an important compound in primary metabolism and a cofactor of many enzymes. In addition, it hydrolyzes (d)NTPs to (d)NMPs and inorganic orthophosphates in a stepwise manner. The structures of YmfB alone and in complex with three sulfates and two manganese ions determined by X-ray crystallography, when compared with the structures of other Nudix hydrolases such as MutT, Ap₄Aase and DR1025, provide insight into the unique hydrolysis mechanism of YmfB. Mass-spectrometric analysis confirmed that water attacks the terminal phosphates of GTP and GDP sequentially. Kinetic analysis of binding-site mutants showed that no individual residue is absolutely required for catalytic activity, suggesting that protein residues do not participate in the deprotonation of the attacking water. Thermodynamic integration calculations show that a hydroxyl ion bound to two divalent metal ions attacks the phosphate directly without the help of a nearby catalytic base.

1. Introduction

Nudix hydrolases are a widespread superfamily present in species ranging from bacteria to humans. In addition, they hydrolyze a wide range of organic pyrophosphates, including (d)NTP (Bhatnagar *et al.*, 1991; Méjean *et al.*, 1994), nucleotide sugars (Lin *et al.*, 2002; Yagi *et al.*, 2003), dinucleoside polyphosphates (Abdelghany *et al.*, 2001; Leslie *et al.*, 2002), dinucleotide coenzymes (Xu *et al.*, 2000) and capped RNAs (Wang *et al.*, 2002). Members of the Nudix hydrolase superfamily have a conserved 23-amino-acid sequence, GX₅EX₇REUXEEXGU (where U is usually Ile, Leu or Val), called the Nudix motif (McLennan, 2006). The glutamate residues in the Nudix signature sequence usually bind divalent metal ions at the active site. The metal ions have the essential role of coordinating the diphosphate of the substrate to be hydrolyzed and the water molecule that attacks the diphosphate (Mildvan *et al.*, 2005).

MutT was the first Nudix enzyme to be discovered; it hydrolyzes the oxidized mutagenic form (8-oxo-dGTP) of dGTP (Abeygunawardana *et al.*, 1995). The *Escherichia coli* *mutT*⁻ strain showed a 1000-fold rise in mutation frequency over the wild type (Yanofsky *et al.*, 1966; Bessman *et al.*, 1996). Based on the antimutator activity of MutT, Nudix hydrolases were initially thought to act in removing potentially toxic compounds from the cell. However, more recently identified Nudix substrates include not only potentially toxic compounds but also various key molecules related to cell signalling and metabolic pathways. Accordingly, Nudix superfamily members are being found to have new roles including RNA processing,

Received 2 December 2013

Accepted 4 February 2014

PDB references: YmfB, 4nfx;
YmfB–Mn–SO₄, 4nfw

Table 1

Data-collection and refinement statistics.

Values in parentheses are for the highest resolution shell. The diffraction data for apo YmfB have previously been published (Hong *et al.*, 2009).

	Apo YmfB	YmfB-Mn-SO ₄
Data collection		
X-ray source	Beamline 17A, KEK	Beamline 4A, PLS
Space group	<i>P</i> 2 ₁	<i>P</i> 4 ₁
Unit-cell parameters (Å, °)	<i>a</i> = 68.9, <i>b</i> = 70.3, <i>c</i> = 145.3, $\alpha = \gamma = 90$, $\beta = 103.2$	<i>a</i> = <i>b</i> = 111.4, <i>c</i> = 247.5, $\alpha = \beta = \gamma = 90$
Wavelength (Å)	0.96405	0.97198
Resolution (Å)	50.00–2.64 (2.73–2.64)	50.00–2.30 (2.34–2.30)
Total reflections	293497	794785
Unique reflections	40006	128765
Completeness (%)	99.7 (99.0)	96.8 (93.1)
Multiplicity	7.3 (7.1)	6.2 (2.9)
<i>I</i> (σ(<i>I</i>))	24.8 (4.5)	8.0 (1.9)
<i>R</i> _{merge} (%)	10.2 (31.6)	14.7 (38.0)
Refinement		
Resolution (Å)	33.56–2.69	32.42–2.30
No. of reflections	35479	122247
<i>R</i> _{work} / <i>R</i> _{free} (%)	23.3/28.8	24.0/28.9
No. of atoms		
Protein	9703	14375
Ligand/ion	—	197
Water	216	334
<i>B</i> factors (Å ²)		
Protein	31.2	33.3
Ligand/ion	—	74.7
Water	31.6	26.0
R.m.s. deviations		
Bond lengths (Å)	0.0042	0.0150
Bond angles (°)	0.8807	1.7815
Ramachandran plot (%)		
Favoured	95.0	92.8
Allowed	4.9	6.6
Disallowed	0.1	0.6
PDB code	4nfx	4nfw

Ca²⁺-channel gating, activation of alcohol dehydrogenase and regulation of ERK signalling (McLennan, 2006).

A novel Nudix hydrolase from *E. coli*, YmfB (molecular mass 17.4 kDa), was cloned and characterized by two different groups (Lawhorn *et al.*, 2004; Xu *et al.*, 2006). The *ymfB* gene was the first gene related to thiamine biosynthesis and degradation to be identified from a genetic screen (Lawhorn *et al.*, 2004). YmfB hydrolyzes thiamine pyrophosphate (TPP) to thiamine phosphate and an orthophosphate. TPP plays a key role in primary metabolism: it serves as a cofactor for many enzymes that catalyze the dehydrogenation of α -keto acids, an essential step in decarboxylation and subsequent conjugation to coenzyme A. YmfB was also found to be a nucleoside triphosphatase and diphosphatase with a broad substrate specificity that releases inorganic orthophosphate in a step-wise manner from the hydrolysis of nucleoside triphosphates instead of the more typical Nudix reaction that releases pyrophosphate in a single step (Xu *et al.*, 2006). Both activities of YmfB agreed with the well known roles of Nudix hydrolase superfamily members such as controlling the intracellular concentration of an essential cofactor or nucleoside phosphate.

The ubiquitous Nudix hydrolase superfamily members have a common catalytic mechanism which requires divalent metal ion(s) to be coordinated by the Nudix motif amino acids and a

phosphate-attacking water molecule to be deprotonated by a nearby catalytic base (Abdelghany *et al.*, 2003). However, the deprotonation mechanism of the attacking water appears to be different in different family members. In *E. coli* MutT the glutamate residue (Glu53) within the Nudix motif was proposed to be both the metal-binding residue and the catalytic base residue (Harris *et al.*, 2000). In the ADP-ribose pyrophosphatases from *E. coli* and *Mycobacterium tuberculosis*, the glutamate residue outside the Nudix motif but located closely to the attacking water in the three-dimensional structure was suggested to be the catalytic base residue (Gabelli *et al.*, 2001; Kang *et al.*, 2003). In addition, although the Nudix motif is strictly conserved in Nudix hydrolase superfamily members, YmfB from *E. coli* and Dr1025 from *Deinococcus radiodurans* (Xu *et al.*, 2001) have an atypical stepwise hydrolysis mechanism of substrate phosphates. In this paper, we present the structure of YmfB from *E. coli* using X-ray crystallography, molecular docking, mass spectrometry, kinetic activity assays of mutant enzymes and thermodynamic integration calculations, and propose a novel metal ion-based catalysis mechanism.

2. Materials and methods

2.1. Site-directed mutagenesis, expression and protein purification

E. coli YmfB was expressed in the T7 vector pET-11a (Novagen) as described previously (Hong *et al.*, 2009). This plasmid was used as a template for site-directed mutagenesis performed using the Muta-Direct site-directed mutagenesis kit (iNtRON Biotechnology) according to the manufacturer's protocols. E23Q, H37A, E51Q, E54Q, E55Q, D98N, D100N and R119A mutants were constructed using the primers in Supplementary Table S1¹. Plasmids were purified from recombinant colonies (QIAprep Spin; Qiagen) and the complete YmfB open reading frame was sequenced on both strands (The Sequencing Service, Macrogen, Seoul, Republic of Korea) to verify the presence of the desired mutation. *E. coli* strain BL21 (DE3) (Novagen) was transformed with wild-type and mutant plasmids. Overexpression and purification of the wild-type and mutant proteins were performed as described for wild-type YmfB (Hong *et al.*, 2009). The purified protein solution contained 20 mM Tris-HCl buffer pH 7.5, 50 mM NaCl and 3 mM β -mercaptoethanol.

2.2. Crystallization and data collection

Crystallization of YmfB was carried out at 283 K via the hanging-drop vapour-diffusion method in 24-well Linbro plates using the Crystal Screen and Crystal Screen 2 screening kits (Hampton Research). Initial thin needle-like crystals were obtained and reproduced in hanging drops comprised of 1 μ l protein solution (8 mg ml⁻¹) mixed with 1 μ l reservoir solution consisting of 0.1 M sodium citrate buffer pH 4.0,

¹ Supporting information has been deposited in the IUCr electronic archive (Reference: DW5088).

3.5% (w/v) PEG 4000, 80 mM magnesium formate. The crystals were improved by streak-seeding, and thicker crystals were obtained in a week with reservoir solution (condition 1) consisting of 0.1 M sodium citrate buffer pH 4.0, 3.5% (w/v) PEG 4000, 64 mM magnesium formate. These crystals were used to determine the structure of the YmfB enzyme, in which no electron density for metal ions was found at the active site. We refer to this YmfB structure as the apo YmfB structure.

To obtain co-crystal structures with substrates or substrate analogues, we searched for new crystallization conditions which did not contain divalent metal ions. A new crystal form was obtained with reservoir solution (condition 2) consisting of 1.4 M ammonium sulfate, 0.1 M MES buffer pH 6.0 in a week. For the YmfB structure with divalent metal ions, we soaked the new YmfB crystals in reservoir solution (condition 2) containing 100 mM MnCl₂.

For data collection, crystals were cryoprotected with the reservoir solution supplemented with 20% glycerol and were flash-cooled to 95 K in liquid nitrogen. Diffraction data were collected on beamline 4A at Pohang Light Source (PLS), Republic of Korea and beamline 17A of the Photon Factory (KEK), Japan. All intensity data were processed and scaled using *HKL-2000* (Table 1).

2.3. Structure determination

The crystal structures of apo YmfB and of YmfB in complex with two Mn²⁺ ions and three sulfate ions (YmfB–Mn–SO₄) were determined with *Phaser* in the *CCP4* package (Winn *et al.*, 2011) using the Nudix hydrolase from *Nitrosomonas europaea* (PDB entry 2b0v; 39% sequence identity; Midwest Center for Structural Genomics, unpublished work) as the search model. The initial solution, optimized by rigid-body refinement, produced clearly interpretable electron density. Manual adjustment of the backbone and side chains was carried out with *Coot* (Emsley *et al.*, 2010).

Of all the attempts to obtain YmfB co-crystal structures with various substrates and divalent metal ions by cocrystallization and soaking methods, suitable crystals were only obtained of a complex with two Mn²⁺ ions and three sulfate ions. The YmfB–Mn–SO₄ structure was determined using the

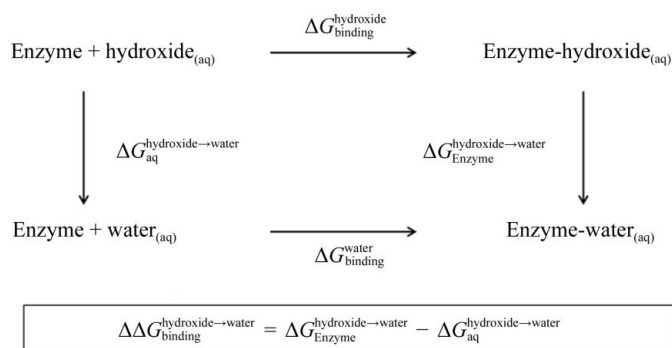


Figure 1

Thermodynamic cycle used to calculate the free-energy cost of exchanging a hydroxide molecule to a water molecule in the active site of the enzyme.

apo YmfB structure as a model. For both structures, after a few rounds of model rebuilding, water molecules were added using $F_o - F_c$ map peaks of $>3.0\sigma$. The R_{free} value was used as an indicator to validate the refinement procedure and to guard against possible overfitting of the data. Stereochemical analysis of the refined structures was performed with *PROCHECK* (Laskowski *et al.*, 1993). Figures were prepared with *PyMOL* (<http://www.pymol.org>). Table 1 summarizes the refinement statistics of the crystal structures.

2.4. Modelling of a YmfB–substrate complex

Docking was performed with the program *ICM* (Abagyan *et al.*, 1994). The YmfB coordinates were used as the receptor for docking the substrates GDP and GTP. Docking was performed on the cavity occupied by sulfate ligands, defined as the space within 5 Å of any ligand atom. Substrate molecules were drawn using the molecule-editor tool from the *ICM* suite and the generated coordinates used for docking. Before docking, all water molecules were removed. Metal ions, which are essential for substrate recognition and hydrolyzing activity, were retained. The structures with the best global energy minima were selected for structural analysis.

2.5. Enzyme-kinetic assays

Each standard reaction mixture of 50 µl consisted of 50 mM Tris pH 8.0, 5 mM MgCl₂, the specified concentration (0, 0.2, 0.4, 0.6, 1.0, 2.0 and 4.0 mM) of GDP or GTP as a substrate and 0.3 µmol YmfB. The inorganic phosphate produced by the enzymatic reaction was quantified using the colorimetric method of Ames & Dubin (1960). Standard measurements for inorganic phosphates were carried out just before the enzyme assays. Each mixture for the enzyme assay was incubated at 310 K for 10 min and the reaction was terminated by the addition of 250 µl 10 mM EDTA and 700 µl Ames solution. Each mixture was incubated at 318 K for 20 min. After the additional incubation, the absorbance at 820 nm of each solution was measured spectrophotometrically. The catalytic activities of the E23Q, H37A, E51Q, E54Q, E55Q, D98N, D100N and R119A mutant proteins were measured using the method used for the wild-type protein. The enzyme-kinetic parameters k_{cat} and K_m were calculated using the nonlinear least-squares fitting program in *GraphPad Prism v.3.02* (GraphPad Software). All measurements were carried out in triplicate. The relative activity was calculated by comparing the catalytic efficiencies (k_{cat}/K_m) of each mutant and the wild type. For mass-spectrometric analysis, the reaction mixture with GTP was prepared using H₂¹⁸O, with 5 mM of GTP as a substrate and 0.3 µmol wild-type YmfB protein.

2.6. LC-ESI-MS/MS analysis

The relevant systems consisted of a 212-LC Binary Solvent Delivery System, a ProStar 410 AutoSampler and a ProStar 335 photodiode-array detector coupled to a 500 Ion Trap mass spectrometer equipped with an electrospray interface (Varian Technologies, Palo Alto, California, USA). A YMC-Pack ODS-AQ column (150 × 4.6 mm) was used at a flow rate of

0.3 ml min⁻¹. The mobile phase consisted of solution *A* [2 mM ammonium acetate in water pH 5.0 (acetic acid)] and solution *B* (2 mM ammonium acetate in 10% aqueous methanol). Samples were run isocratically with solution *A* at 100%(v/v) for 5 min and a linear gradient to 30% solution *B* for 30 min, held at 100% solution *B* for 45 min and then decreased linearly to 0% solution *B* over 45 min and held for 50 min for the next analytical sample. A 10 µl aliquot of each fraction was subsequently injected into an HPLC system.

The system was operated under the *MS Workstation* software (v.6.9; Varian). Mass spectra were acquired using an electrospray ionization (ESI) source in negative-ionization mode. The full-scan mass spectra were recorded over the *m/z* range 100–800. The operating parameters in the positive-ion mode were as follows: a spray needle voltage of 6 kV, a

capillary voltage of 72 V, a drying temperature of 623 K, a drying gas pressure (nitrogen) of 172 kPa, a nebulizer gas pressure (air) of 345 kPa and helium as the neutral collision gas. MS/MS analysis results were analyzed using Turbo Data-Dependent Scanning (TurboDDs). The collision-induced dissociation (CID) voltage was automatically set by TurboDDs. Data were acquired in continuous mode within a mass scan of 15 000 u s⁻¹. The mass scan average was set at three microscans (4.37 s per scan).

2.7. Thermodynamic integration calculations

Thermodynamic integration calculations were carried out to compute the free energy of exchanging a hydroxide ion bound to the two metals with a water molecule. The simulations involved two transformations: the conversion of a hydroxide ion into a water molecule in a periodic box with bulk water and the same transformation with the molecules to be converted bound to the metal ions in the active centre of the enzyme. Fig. 1 depicts the thermodynamic cycle used to calculate the free energy of exchange.

Explicit TIP3P water molecules were used (Jorgensen *et al.*, 1983) in a periodic box with margins of 12 Å beyond the hydroxide ion or beyond the protein; starting sizes were 74 × 61 × 74 Å for the enzyme system and 31 × 31 × 30 Å for the hydroxide ion in solution. The short-range van der Waals interactions were truncated at 10 Å. Coulombic interactions were taken into account with the PME method and a cutoff of 10 Å for the real part of the sum (Essmann *et al.*, 1995). Each transformation was performed in two stages, each with the transformation of the force-field potential divided into nine steps (with even increments between 0 and 1). Simulations of 1 ns were run for each of the nine steps. The first stage corresponded to the modification of the atomic charges of the O and H atoms to their respective charges in TIP3P water. The second stage corresponded to the addition of the atomic charge of the missing H atom. As TIP3P water H atoms do not have van

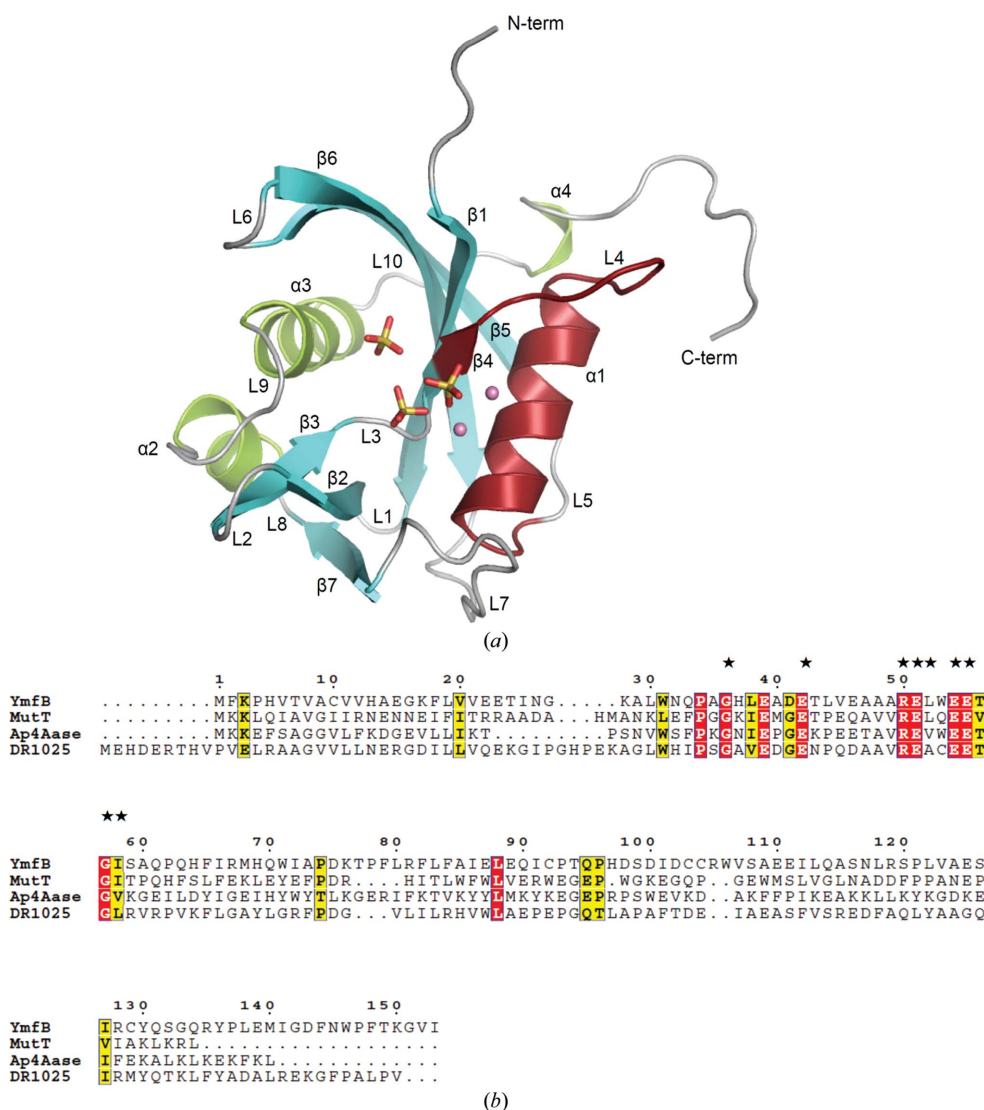


Figure 2 Overall structure of YmfB from *E. coli*. (a) Ribbon diagram showing the overall fold of the YmfB–Mn–SO₄ structure with α -helices and β -strands shown as yellow-green coils and cyan arrows, respectively, apart from the Nudix motif, which is highlighted in red. Three sulfates and two Mn²⁺ ions are represented as sticks and spheres, respectively. All helices, strands and loops, including the N-terminus and C-terminus, are labelled. (b) A structure-based sequence alignment of YmfB with the other Nudix hydrolases MutT, Ap₄Aase and DR1025. Conserved residues are shown as white letters in red boxes. Conservative substitutions are placed in yellow boxes. Starred residues represent the Nudix signature sequence.

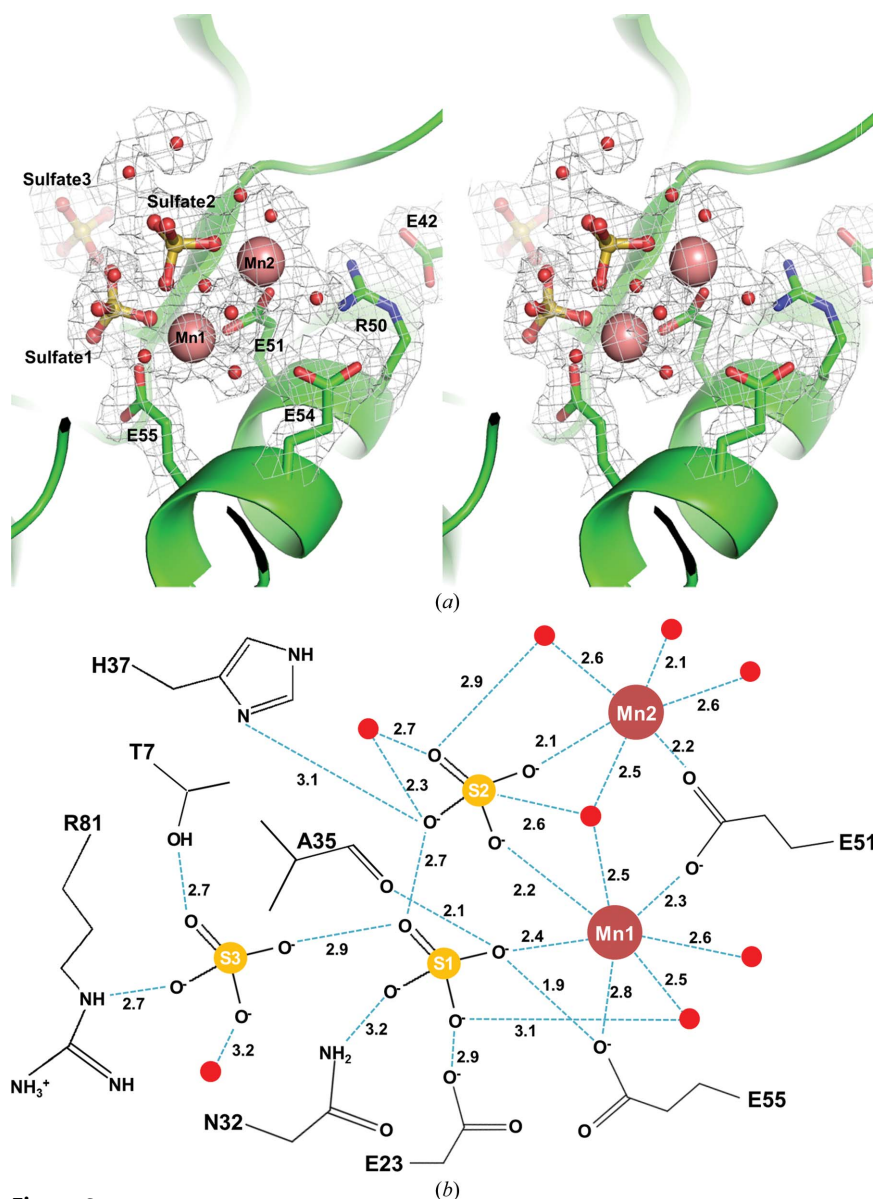


Figure 3
 Binding site for Mn^{2+} ions and sulfate anions. (a) A stereoview of the binding site between the Mn^{2+} ions and sulfate anions above the Nudix helix. Three bound sulfate anions are depicted in ball-and-stick representation; associated Mn^{2+} cations (salmon spheres), water molecules (red spheres) and coordinating amino-acid residues are also shown. (b) Detailed view of the coordination scheme in the ligand-binding site. The interactions between protein residues and ligands are shown by cyan dashed lines with distances indicated in angstroms. Water molecules are shown as red balls.

der Waals parameters, this is sufficient to create the H atom. We used previously published parameters for the hydroxide (Pang, 2001), the sulfate molecules (Kirschner *et al.*, 2008) and the manganese metal ions (Bradbrook *et al.*, 1998). Simulations were performed with the AMBER 10 software (Case *et al.*, 2008).

3. Results

3.1. Crystal structure of YmfB

Size-exclusion chromatography studies suggest that YmfB exists as a monomer in solution. In the crystal packing of apo

YmfB, four dimers of YmfB were present in the asymmetric unit, while in the metal-bound YmfB crystal six dimers of YmfB were present in the asymmetric unit. The YmfB structure has the Nudix fold, which comprises three mixed layers $\alpha/\beta/\alpha$ including a central β -grasp motif (Murzin *et al.*, 1995; Fig. 2a). Two α -helices (helices $\alpha 1$ and $\alpha 4$) compose the first α layer. The central β layer consists of seven β -strands (strands $\beta 1$, $\beta 2$, $\beta 3$, $\beta 4$, $\beta 5$, $\beta 6$ and $\beta 7$). Two α -helices (helix $\alpha 2$ and $\alpha 3$) compose the last α layer. The Nudix box spans from strand $\beta 4$ to helix $\alpha 1$ including loop 4 (strand-loop-helix). Residues Gly133–Lys150 wrap around the core Nudix fold as a loop and a short helix $\alpha 4$ at the opposite side of the substrate-binding cleft (Fig. 2b).

3.2. Metal binding

To investigate the atypical hydrolysis mechanism, we tried to identify metal-binding residues in the conserved active site of other Nudix enzymes. Glutamates of the Nudix signature sequence play a key role in coordinating the metal ion(s) in most cases, and in YmfB all of the Nudix signature residues are conserved (Fig. 2b). Although YmfB crystals were obtained using a reservoir solution containing 64 mM magnesium formate, at the pH of the buffer (pH 4.0) magnesium ion was not present in the YmfB structure. Since the pK_a of the side chain of glutamate is ~ 4.2 at pH 4.0, the putative metal-coordinating glutamates of the Nudix motif are probably protonated and therefore not active for metal binding. To find the position of the ion(s), other crystallization conditions were screened, and different YmfB crystals were obtained with a reservoir solution consisting of 1.4 M ammonium sulfate, 0.1 M MES buffer pH 6.0. These YmfB crystals were soaked in reservoir solution with the addition of 100 mM

MnCl_2 . Distinct extra density was found at the active site in the unbiased isomorphous difference Fourier ($F_o - F_c$) map generated using the apo YmfB structure (Fig. 3a and Supplementary Fig. S1). Two manganese ions were bound by two glutamate residues, Glu51 and Glu55, which are both Nudix signature residues. Extra densities corresponding to three sulfate anions were also present; the first and second sulfates were coordinated by two bound manganese ions at the active site. The first manganese ion (Mn1) was coordinated, with short distances, to seven groups: two sulfate O atoms (2.18 and 2.35 Å), the carboxylate groups of Glu51 (2.33 Å) and Glu55 (2.76 Å), and three water molecules (2.47, 2.47 and

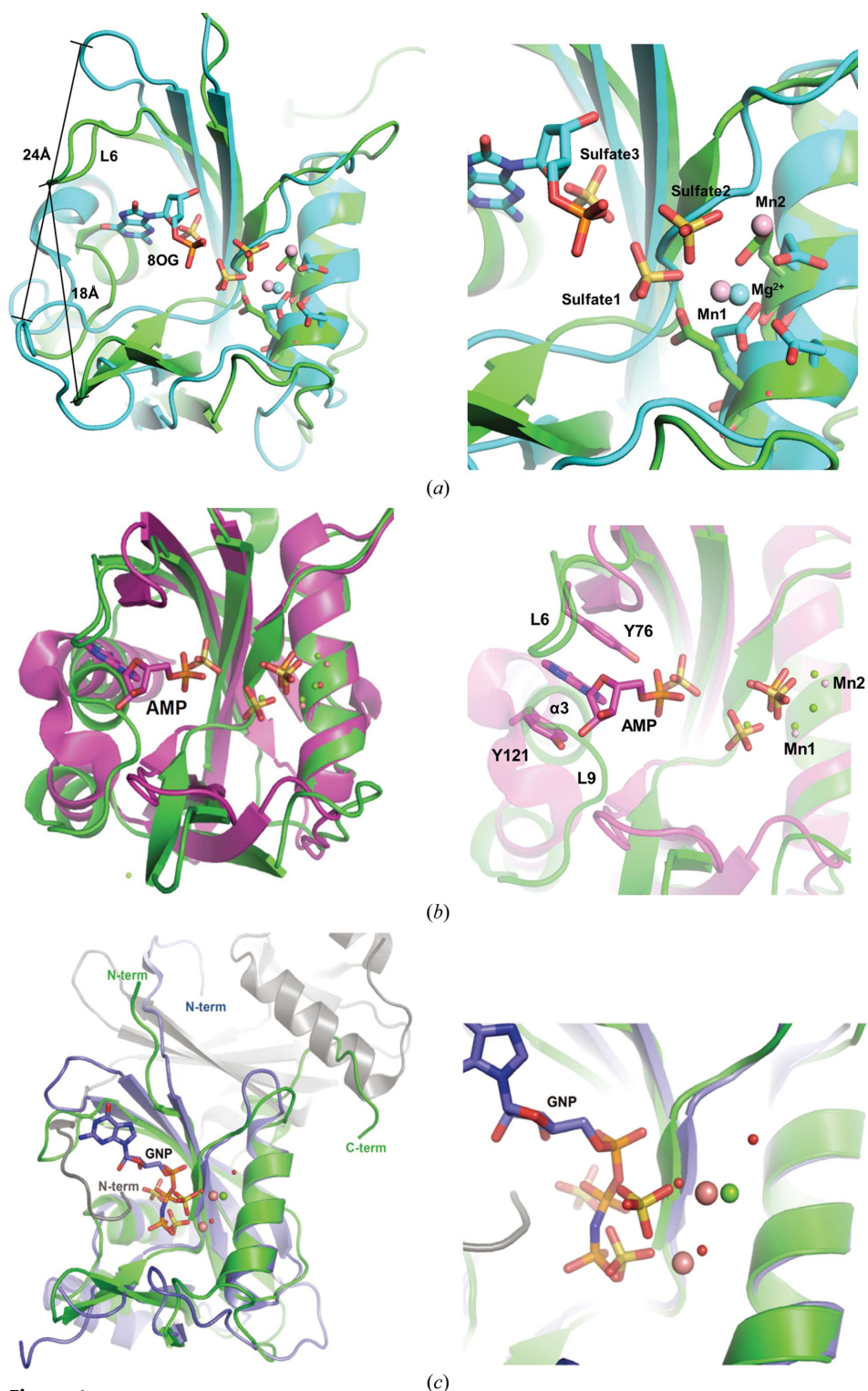


Figure 4
 Structural comparison between YmfB and other representative Nudix hydrolases performed using *DALI*. (a) Superposition of YmfB (green) and MutT (cyan) with bound ligands. Sulfates and Mn^{2+} ions (salmon spheres) are ligands of YmfB, and 8-oxo-2'-deoxy-guanosine-5'-monophosphate (8OG) and Mg^{2+} ion (cyan sphere) are ligands of MutT. Loop6 (L6) of YmfB is labelled. The distances between L6 and loop9 (L9) of YmfB and MutT are indicated by black lines. The distance in YmfB is 18 Å; that in MutT is 24 Å. (b) Superposition of YmfB (green) and Ap_4Aase (magenta) with bound ligands. Sulfates and Mn^{2+} ions (salmon spheres) are ligands of YmfB, and AMP; Mg^{2+} ions (green spheres) and phosphate are ligands of Ap_4Aase . (c) Superposition of YmfB (green) and DR1025 (slate and grey) with bound ligands. Sulfates and Mn^{2+} ions (salmon spheres) are ligands of YmfB and phosphaminophosphonic acid-guanylate ester (GNP), Mg^{2+} ion (green sphere) and waters (red spheres) are ligands of DR1025. Each terminus of both proteins is in the same colour as the backbone.

2.56 Å) (Fig. 3b). The second manganese ion ($Mn2$) was coordinated to six groups in an octahedral arrangement: one sulfate O atom (2.14 Å), the carboxylate of Glu51 (2.18 Å), and four water molecules (2.14, 2.48, 2.55 and 2.63 Å). Three sulfate anions were observed in the substrate-binding pocket (SBP). The first sulfate (Sulfate1) was coordinated by the side chains of Glu23, Asn32 and Glu55, the main chain of Ala35, $Mn1$, the other two sulfates and water molecules. The second sulfate (Sulfate2) was coordinated by the side chain of His37, $Mn1$ and $Mn2$, and by Sulfate1 and water molecules. The third sulfate (Sulfate3) was located deep inside the SBP and was coordinated by the side chains of residues Thr7 and Arg81, Sulfate1 and a water molecule. When we compared the metal-bound YmfB structure with the apo YmfB structure, the overall conformations were well conserved. The two metal-binding residues Glu51 and Glu55 had the same side-chain conformation regardless of divalent metal binding at the active site (Supplementary Fig. S1). The nearby negatively charged residues Glu23, Asp98 and Asp100 showed more flexible conformations.

3.3. Structural comparison with other Nudix hydrolases

YmfB has a broad substrate specificity for nucleoside phosphates (Xu *et al.*, 2006). Significant structural homology (*DALI* server; Holm *et al.*, 2006) was found with the *N. europaea* Nudix hydrolase (*Z*-score = 21.8; PDB entry 2b0v), Ap_6A hydrolase (*Z*-score = 16.8; PDB entry 1vc8; RIKEN Structural Genomics/Proteomics Initiative, unpublished work), an 8-oxo-dGTPase domain (*Z*-score = 16.7; PDB entry 2yyh; RIKEN Structural Genomics/Proteomics Initiative,

unpublished work) and DR1025 (Z -score = 16.4; PDB entry 1sz3; Ranatunga *et al.*, 2004). The substrates of these structural homologues included GTP analogues and Ap_nA . We selected three representative Nudix hydrolases in complex with their substrates from the list, and the YmfB–Mn– SO_4 structure was compared with the structures of MutT in complex with 8-oxo-dGMP (Harris *et al.*, 2000; Lin *et al.*, 1997), of Ap_4Aase in complex with AMP (Bailey *et al.*, 2002) and of DR1025 in complex with phosphoaminophosphonic acid-guanylate ester (GNP) (Ranatunga *et al.*, 2004). The C^α positions of the Nudix helix and bound metal sites were used to verify the aligned structures. The three Nudix hydrolases require a different number of divalent metal ions for their enzymatic activities, and their most favoured substrates have different numbers of phosphates.

MutT is a nucleoside triphosphate pyrophosphatase that converts (d)NTPs into (d)NMPs and PP_i (Bhatnagar & Bessman, 1988). Both YmfB and MutT are monomeric proteins, and the r.m.s.d. between the two structures is 2.74 Å for 109 C^α atoms. The central β layer in the Nudix fold generally consists of two β -sheets: $\beta 4/\beta 1/\beta 6/\beta 5$ and $\beta 7/\beta 2/\beta 3$ in YmfB. The cleft between the two β -sheets is the conserved SBP of the Nudix hydrolase superfamily. The most noticeable difference between YmfB and MutT is that YmfB has a close conformation of the two β -sheets. The width between the two ends of the β -sheets in YmfB was 18 Å, compared with 24 Å in

MutT. As a consequence, the SBP of YmfB is narrower than that of MutT (Fig. 4*a*). The position of the MutT magnesium ion superimposes on that of Mn1, and the α -phosphate of 8OG is positioned close to Sulfate3 of YmfB.

Ap_4Aase is a dinucleotide polyphosphatase that cleaves Ap_4A asymmetrically into ATP and AMP (Conyers *et al.*, 2000). The overall fold of YmfB and Ap_4Aase is similar except that YmfB has extra residues at the C-terminus. Both exist as monomers, and the r.m.s.d. between the two structures is 1.82 Å with 113 C^α atoms aligned. Of the four magnesium ions found in the active site of the Ap_4Aase –AMP– PO_4 structure, two are at the same positions as occupied by Mn1 and Mn2 in YmfB. The Ap_4Aase phosphate is almost at the same position as Sulfate2. The Ap_4Aase AMP is bound deeply inside the SBP, and the adenine is tightly stacked between Tyr76 of loop6 (L6) and Tyr121 of loop9 (L9) of Ap_4Aase . However, L6 and L9 of YmfB are longer and helix $\alpha 3$ is located deeper inside the SBP. The resulting base-recognition pocket between L6 and L9 of YmfB is closed (Fig. 4*b*). Thus, shorter substrates such as (d)NTP and (d)NDP could be more suitable for binding to YmfB. The α -phosphate of AMP is located next to Sulfate3.

DR1025 from *D. radiodurans* is both a nucleoside triphosphatase and a dinucleotide polyphosphatase, and was the first Nudix hydrolase found to hydrolyze two different classes of substrates (Xu *et al.*, 2003). DR1025 exists as a homodimer

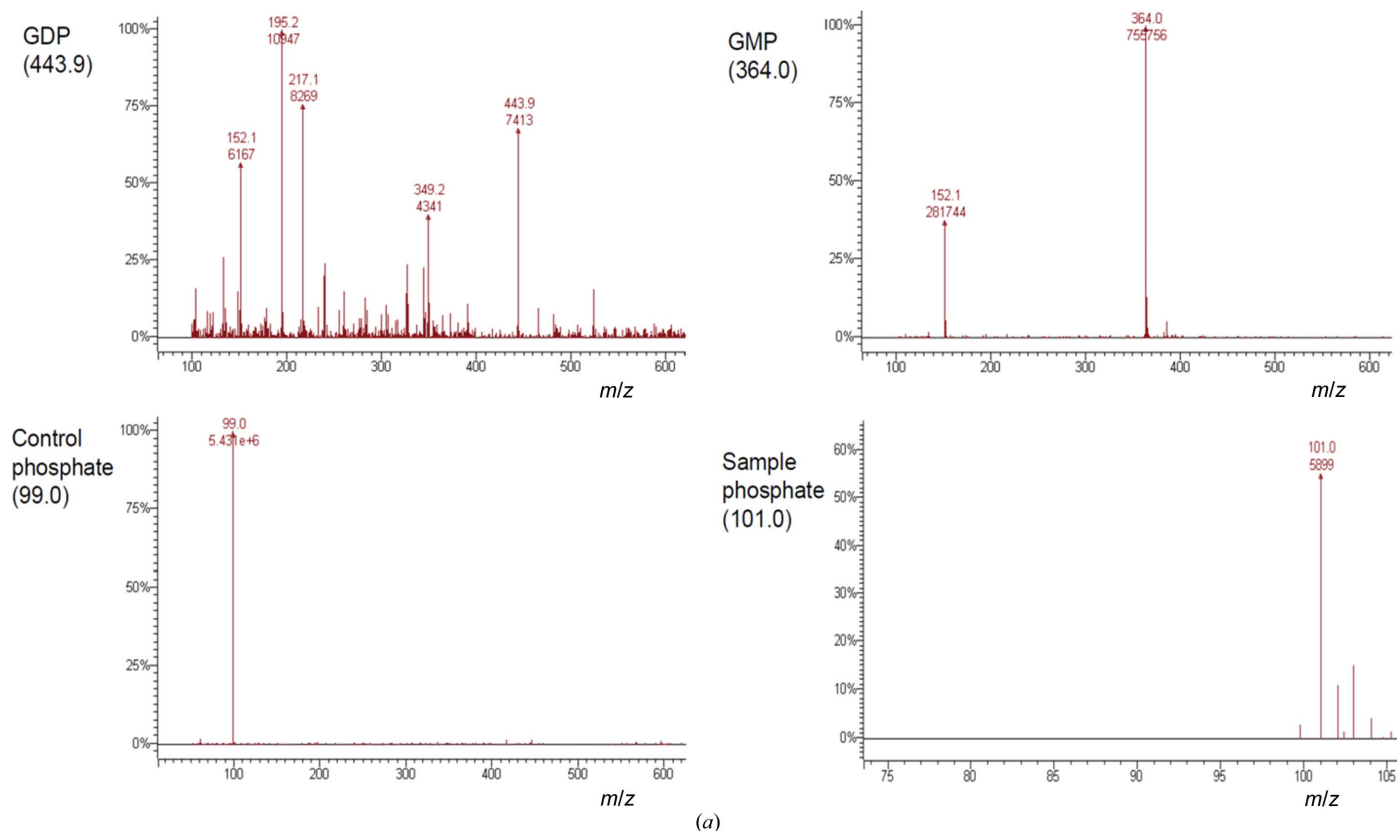


Figure 5

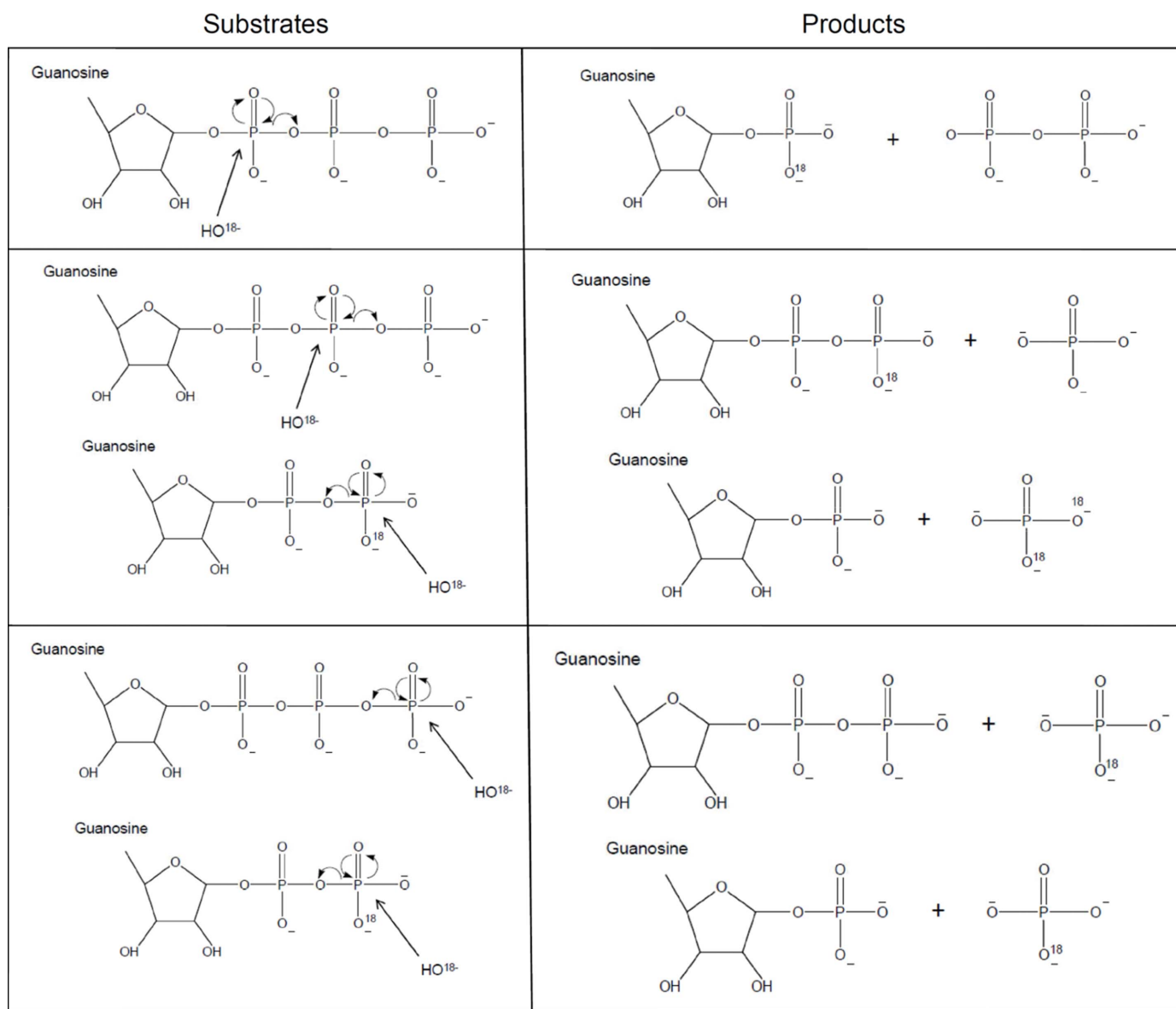
Mass-spectrometric results and the proposed mechanism of GTP hydrolysis. (a) Mass-spectrometric results of phosphate ion as a control and detected masses of GDP, GMP and sample phosphate from a sample of the GTP hydrolysis reaction in H_2^{18}O .

that swaps N-terminal segments between adjacent monomers. The r.m.s.d. between DR1025 and YmfB is 2.26 Å for the 133 C α atoms aligned. DR1025 complex structures showed one or three divalent metal ions in each monomer depending on whether the bound ligand was GNP or ATP. YmfB is a monomeric protein, and the longer C-terminus (Gln134–Ile153) occupies the dimer-interface position of DR1025 (Fig. 4c). Although the overall SBPs of YmfB and DR1025 are well conserved, in DR1025 the N-terminal extension (Met1–Pro10) from monomer *B* is involved in substrate recognition at the active site of monomer *A*. The γ - and β -phosphates of bound GNP and the magnesium ion in the DR1025–GNP complex occupy positions similar to those of

Sulfate1, Sulfate2 and Mn2 in the YmfB complex structure, respectively.

3.4. Mass-spectrometric analysis of the GTP hydrolysis reaction in ^{18}O water

To elucidate the atypical hydrolysis mechanism of YmfB, we carried out the GTP-hydrolysis reaction in ^{18}O water and analyzed the reaction products by tandem mass spectrometry (MS/MS). The solution contained GDP and GMP without any ^{18}O atoms, and all phosphate anions were orthophosphate and only contained an ^{18}O atom (Fig. 5a). No pyrophosphate anion was detected, confirming that YmfB hydrolyzed GTP into orthophosphate only in a stepwise manner.



(b)

Figure 5 (continued)

(b) Three different proposed mechanisms of GTP hydrolysis. The first line depicts the hydrolysis mechanism of GTP by attack on the α -phosphate by an H_2^{18}O molecule. The second line depicts the hydrolysis mechanism of GTP and GDP by attack on the β -phosphate by an H_2^{18}O molecule. The third line depicts the hydrolysis mechanism of GTP and GDP by attack on the γ -phosphate and the β -phosphate by an H_2^{18}O molecule, respectively. The products of each reaction are shown in the right column. The results in (a) indicate that the third mechanism is operational in hydrolysis by YmfB.

Table 2

Kinetic data of YmfB mutants for GDP and GTP.

To obtain averaged relative activity and kinetic parameters, all experiments were performed three times.

	Relative activity† (%)		GDP			GTP		
	GDP	GTP	K_m (mM)	k_{cat} (min ⁻¹)	k_{cat}/K_m (mM ⁻¹ min ⁻¹)	K_m (mM)	k_{cat} (min ⁻¹)	k_{cat}/K_m (mM ⁻¹ min ⁻¹)
WT	100.0	100.0	1.6 ± 0.1	(5.3 ± 0.2) × 10 ⁻²	(3.3 ± 0.4) × 10 ⁻²	2.2 ± 0.3	(5.2 ± 0.4) × 10 ⁻²	(2.4 ± 0.5) × 10 ⁻²
E23Q	9.4	16.3	2.0 ± 0.5	(6.2 ± 0.8) × 10 ⁻³	(3.4 ± 1.3) × 10 ⁻³	3.5 ± 0.7	(1.3 ± 0.2) × 10 ⁻²	(4.0 ± 1.4) × 10 ⁻³
H37A	55.9	89.5	2.0 ± 0.3	(3.7 ± 0.3) × 10 ⁻²	(1.9 ± 0.5) × 10 ⁻²	2.0 ± 0.2	(4.2 ± 0.2) × 10 ⁻²	(2.1 ± 0.3) × 10 ⁻²
E51Q‡	N/A	N/A	N/A	N/A	N/A	N/A	N/A	N/A
E54Q	73.6	46.8	1.9 ± 0.4	(4.5 ± 0.5) × 10 ⁻²	(2.5 ± 0.8) × 10 ⁻²	0.6 ± 0.1	(6.7 ± 1.0) × 10 ⁻³	(1.1 ± 0.2) × 10 ⁻²
E55Q‡	N/A	N/A	N/A	N/A	N/A	N/A	N/A	N/A
D98N	54.3	18.5	1.0 ± 0.2	(1.7 ± 0.1) × 10 ⁻²	(1.8 ± 0.5) × 10 ⁻²	1.2 ± 0.2	(5.5 ± 1.0) × 10 ⁻³	(4.9 ± 1.7) × 10 ⁻³
D100N	54.5	55.0	1.6 ± 0.2	(2.9 ± 0.2) × 10 ⁻²	(1.9 ± 0.4) × 10 ⁻²	2.1 ± 0.2	(2.8 ± 0.1) × 10 ⁻²	(1.4 ± 0.2) × 10 ⁻²
R119A	22.4	40.0	3.8 ± 0.6	(2.8 ± 0.3) × 10 ⁻²	(7.7 ± 0.2) × 10 ⁻³	3.6 ± 0.2	(3.5 ± 0.2) × 10 ⁻²	(9.8 ± 1.1) × 10 ⁻³

† This relative activity (%) is derived from k_{cat}/K_m . ‡ No enzymatic activity was detected for these mutants.

Among the α -, β - and γ -phosphates of GTP, if the α -phosphate of GTP is attacked by ¹⁸O water the resulting GMP would have an ¹⁸O atom and a pyrophosphate would be released (Fig. 5*b*, top). Neither of these, however, was found in the reaction solution. If ¹⁸O water attacks the β -phosphate of GTP and the β -phosphate of GDP sequentially, the released orthophosphate anions should be a mixture of 50% phosphate anions with two ¹⁸O atoms and 50% phosphate anions with no ¹⁸O atom (Fig. 5*b*, middle). Again, neither of these products were found in the resulting solution. If ¹⁸O water attacks the γ -phosphate of GTP and the β -phosphate of GDP sequentially, all released orthophosphate anions should have an ¹⁸O atom among the four O atoms (Fig. 5*b*, bottom). The result of our MS/MS study supports the third mechanism and proves that the water only attacks the end phosphate of the substrates: the γ -phosphate of GTP and the β -phosphate of GDP.

3.5. Molecular docking: YmfB–Mn–GDP complex

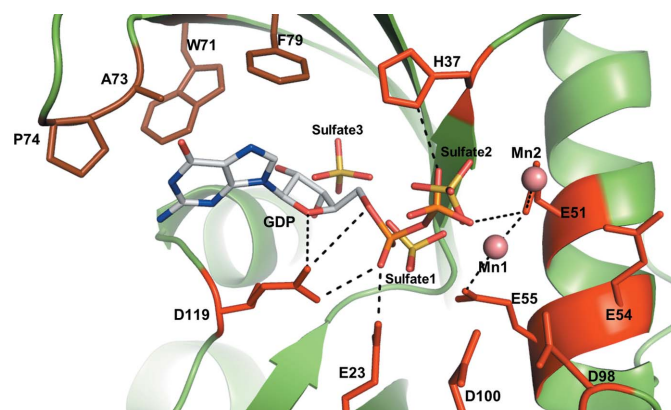
We tried to obtain substrate-bound or substrate analogue-bound cocrystal structures using both crystallization conditions. The crystals obtained by soaking or co-crystallization with substrates or substrate analogues showed no distinct extra density in the active site for the soaked ligands. However, the positions of Mn²⁺ and sulfate ions in the YmfB–Mn–SO₄ complex agreed with the positions of metal ions and phosphates of bound substrates in other Nudix hydrolases. Using this information, we used molecular docking to generate models of substrates bound to YmfB. The YmfB–Mn–SO₄ structure was used as the platform to dock substrates, and the positions of the Mn²⁺ and sulfate ions were used to verify the models.

The β -sheet ($\beta_4/\beta_1/\beta_6/\beta_5$) in the upper wall SBP of YmfB is lined with the hydrophobic residues Trp71, Ala73, Pro74 and Phe79. In the YmfB–Mn–GDP model, the guanine base of GDP interacts with Trp71, Ala73 and Phe79 (Fig. 6). Arg119 from L9 forms hydrogen bonds to the α -phosphate and the O atom of the ribose ring. The β -phosphate is coordinated by Mn1, Mn2 and His37, and the α -phosphate by Glu23, Asn32, Ala35 and Arg119. The positions of the α - and β -phosphates of GDP were similar to the positions of Sulfate1 and Sulfate2

in the YmfB–Mn–SO₄ structure. The position of the ribose moiety of GDP is close to that of Sulfate3. The phosphate-binding pocket (PBP) near Mn1 and Mn2 is mostly covered by the side chains of the acidic residues Glu23, Asp98 and Asp100, in addition to Asp51, Asp54 and Asp55 of the Nudix signature sequence. The PBPs of YmfB and DR1025 have a broader negatively charged area compared with those of MutT and Ap₄Aase (Fig. 7), in which the diphosphate of the substrate would be hydrolyzed by water.

3.6. Characterization of active-site mutants

To determine their contribution to the catalytic mechanism, we performed site-directed mutagenesis of residues thought to interact with substrates. Kinetic analysis was used to characterize mutants of the Glu51 and Glu55 residues that directly coordinate Mn1 and Mn2, and another four acidic residues Glu23, Glu54, Asp98 and Asp100 located in the PBP close to the metal ions were also chosen for mutation. The residues His37 and Arg119, which coordinate the β - and α -phosphates of substrates in the model structures, were also identified. We mutated all of these residues and studied their kinetic para-

**Figure 6**

Molecular-docking model of YmfB with GDP. The docked GDP molecule is superimposed onto the YmfB–Mn–SO₄ structure. Directly interacting residues are labelled and hydrogen-bond interactions are indicated as dotted lines. Residues making van der Waals interaction with the guanine of GDP are shown in brown. Residues mutated for enzyme-kinetic studies are labelled in red.

Table 3

Results of the thermodynamic integration calculations.

 All values are in kcal mol⁻¹.

Hydroxide→ water	Transformation in solvent	Transformation in the enzyme	$\Delta\Delta G$
Stage 1	102.32	114.99	12.7
Stage 2	22.65	24.46	1.8
Sum	124.98	139.45	14.5

meters for the hydrolysis of GTP and GDP (Table 2). The correlations (R^2) for the nonlinear least-squares fit of k_{cat} and K_{m} are shown in Supplementary Table S2. We confirmed that less than 20% of the substrate was hydrolyzed in all reaction assays.

The E51Q and E55Q mutants showed no detectable hydrolytic activity for either substrate, implying that the two metal ions are essential for hydrolysis. It is well established in the Nudix hydrolase family that the divalent metal ions bound by the Nudix signature residues directly interact with the substrate diphosphate and also coordinate the water molecule that attacks the diphosphate. In the YmfB–Mn–SO₄ structure two manganese ions bind Sulfate1 and Sulfate2, and coordinate a water molecule in a good position to attack a putative phosphate at the position of Sulfate2 (Fig. 3*b*). The dual role

of the metal ions in recognizing a substrate and coordinating the attacking water molecule explains why the E51Q and E55Q mutations result in no detectable catalytic activity.

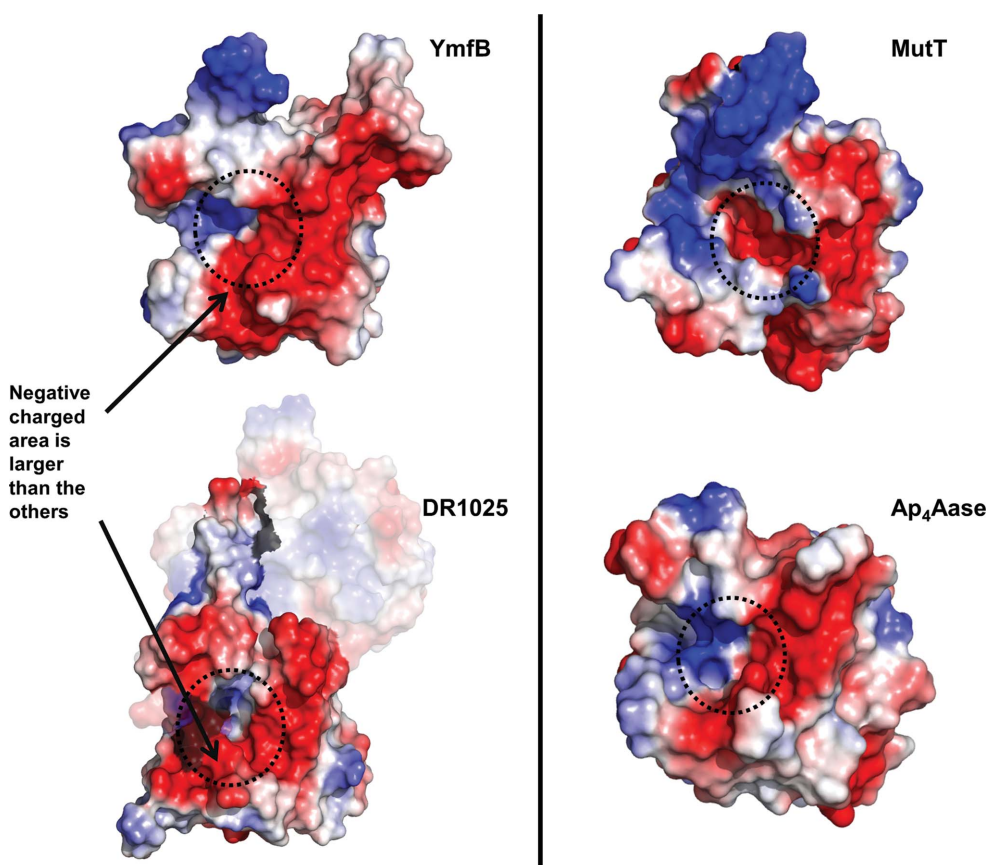
Residue Glu23 makes a hydrogen bond to Sulfate1, which occupies the putative position of the α -phosphate of GDP. Mutation of Glu23 to glutamine results in a greater than 80% reduction in hydrolytic activity for both substrates. Residue Arg119, located next to Glu23, also makes hydrogen bonds to Sulfate1. The positively charged guanidium group of Arg119 could stabilize the negative charge of the α -phosphate of the leaving GMP after the hydrolysis of GDP. The R119A mutant showed a greater than 50% activity loss for both GTP and GDP. His37 coordinates Sulfate2 by a hydrogen bond, and the H37A mutant showed 10–40% activity loss for both substrates.

The effect of the mutations on the hydrolytic activity is substrate-specific. The E23Q, H37A and R119A mutants showed lower catalytic activity for GDP than GTP, but the E54Q and D98N mutants showed the opposite trend: the catalytic activity of E54Q and D98N for GTP is lower than that for GDP. The carboxylates of both Glu54 and Asp98 are located more than ~ 4 Å away from sulfates or metal ions, and do not interact directly with them. The E54Q mutant showed 53 and 26% activity loss towards GTP and GDP, respectively. The D98N mutant showed 82 and 45% activity loss towards GTP and GDP, respectively. These results suggest that both

residues are more involved in the hydrolysis of GTP than that of GDP. Residue Asp100 is also located far from sulfates and metal ions, but its position is not in line with the putative phosphate-binding and metal-binding sites. The D100N mutant lost approximately 45% activity for both substrates. We also measured the catalytic hydrolysis activity of YmfB for TPP. The activity for TPP was 27% of that for GDP.

3.7. Characterization of the solvent species bound to the two metals: mechanistic implications

The results of site-directed mutagenesis suggested that none of the residues in the active site are absolutely required for the deprotonation of the water molecule that attacks the substrate phosphates. Therefore, we evaluated the possibility that the species bound to the two metal ions is already deprotonated, *i.e.* a hydroxide ion. Thermodynamic integration calculations showed that it is


Figure 7

Surface potential representations of YmfB and other compared Nudix hydrolases. Positive surface potential is represented in blue and negative surface potential in red. The substrate-binding pockets of each protein are indicated as dotted circles.

much more probable to have a hydroxide ion bound to the two manganese ions than a water molecule (Table 3). The standard molar free energy ($\Delta^\circ G_1$) associated with the exchange of a metal-bound water by a bulk hydroxide corresponds to the standard Gibbs energy of the reaction

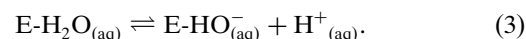
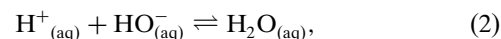


and its value was calculated as $-14.5 \text{ kcal mol}^{-1}$ (equilibrium constant of 1.6×10^{10}). The energies for all of the calculation steps are shown in Table 3. We also found that upon converting the hydroxide to water, the molecule loses its coordination to one of the metals. This result further indicates that the coordination of a water molecule to the two metal

ions is not as stable as the same coordination to a hydroxide ion.

The reaction energy at neutral pH can be calculated by considering the real, non-standard, physiological concentrations of water ($55.14 \text{ mol dm}^{-3}$ at 310 K; Tanaka *et al.*, 2001) and hydroxide ($1.54 \times 10^{-7} \text{ mol dm}^{-3}$ at neutral pH and 310 K; Marshall & Franck, 1981). Substituting these values in the equilibrium-constant equation, we obtain an $[\text{E-HO}^-]/[\text{E-H}_2\text{O}]$ ratio of approximately 46. This means that under physiological conditions, the free energy of reaction is $-2.4 \text{ kcal mol}^{-1}$. This still favours the binding of hydroxide to the active-site metals instead of water, despite the enormous difference in their concentration. It is still much more probable to find a hydroxide ion than a water molecule bound to the metals in the active centre.

One interesting point of the thermodynamic calculations is that they allow the calculation of the $\text{p}K_a$ of the metal-bound water molecule. Reaction (1) can be decomposed into the sum of two acid-ionization reactions:



The first reaction represents the reverse of the ionization of a water molecule in bulk water and the second reaction represents the ionization of metal-bound water inside the enzyme active site. Therefore, $\Delta^\circ G_1$ corresponds to the difference in free energy of these two acid-ionization reactions [calculated as $\Delta^\circ G_2 + \Delta^\circ G_3$ for (2) and (3), respectively]. As the $\text{p}K_a$ of a molecular species can be calculated from the standard Gibbs energy of ionization ($\Delta^\circ G_{\text{ioniz}} = 2.303RT\text{p}K_a$), then the reaction free energy for reaction (1) can be related to the difference in $\text{p}K_a$ between the bulk water molecules and the active site metal-bound water molecule (Simonson *et al.*, 2004; Warshel *et al.*, 1986):

$$\text{p}K_a(\text{bulk water}) - \text{p}K_a(\text{metal-bound water}) = \frac{\Delta^\circ G_1}{2.303RT}. \quad (4)$$

At 310 K water has an ionization constant (K_w) of 2.4×10^{-14} (Marshall & Franck, 1981), which results in a $\text{p}K_a$ for water molecules in bulk water of 15.4. Introducing this value into (4) we obtain a $\text{p}K_a$ for the metal-bound water of 5.2.

4. Discussion

Many Nudix hydrolases have been studied for their biological roles and enzymatic activities (Mildvan *et al.*, 2005; McLennan, 2006). The hydrolysis mechanism of the Nudix hydrolase superfamily is well conserved in the way that the water, coordinated by a divalent metal ion(s), is deprotonated by a catalytic base (a glutamate or histidine residue) and the resulting OH^- ion attacks the phosphate or the carbon of the sugar ring as a nucleophile, leading to hydrolysis of the substrate. The divalent metal ion(s) are essential for the hydrolysis activity of the Nudix hydrolases, and the number of bound metal ion(s) at the active site varies depending on the

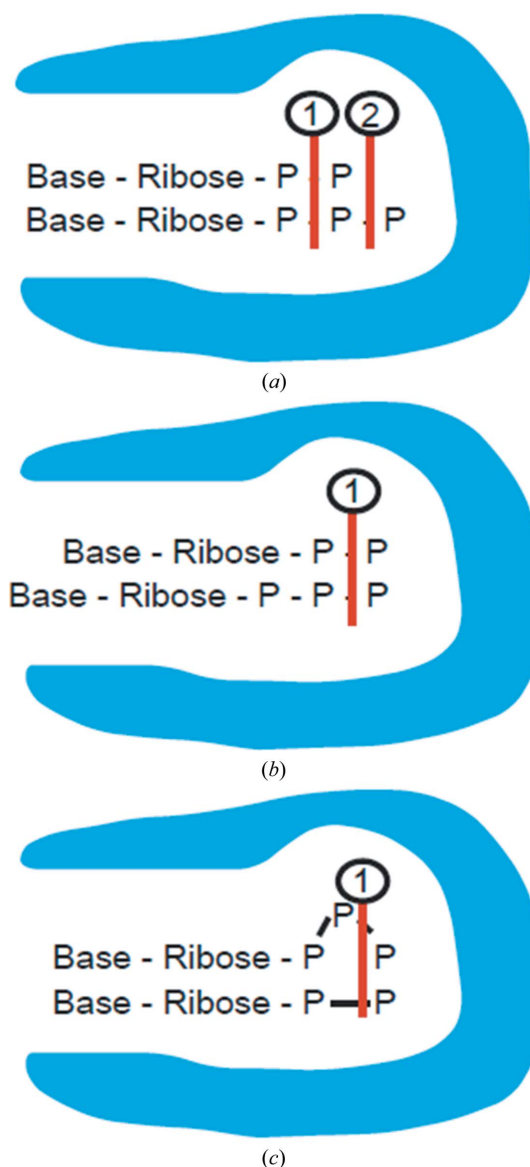


Figure 8 Three possible mechanisms of hydrolysis of (d)NTP into (d)NMP and two orthophosphates. (a) Hydrolysis mechanism with two attacking sites. (b) Hydrolysis mechanism with one attacking site in the substrate-binding shift model. (c) Hydrolysis mechanism with one attacking site in the flexible-substrate phosphate-binding model.

Nudix hydrolase: MutT has two metal ions (Frick *et al.*, 1994), ADPRase three (Kang *et al.*, 2003; Gabelli *et al.*, 2002), Ap₄Aase three (Conyers *et al.*, 2000) and GDPMHase one (Legler *et al.*, 2002). YmfB is unique in that it releases inorganic orthophosphate from the hydrolysis of triphosphates in a stepwise manner, instead of releasing pyrophosphate (Xu *et al.*, 2006). YmfB has an atypical activity in that it hydrolyzes the triphosphate of (d)NTPs in a stepwise manner. From MS/MS results we determined that a water molecule always attacks the end phosphate of the substrates.

An interesting question is how many catalytic sites exist in YmfB to account for its atypical activity. To hydrolyze the phosphates of (d)NTPs one by one, YmfB could have one attacking site or two different attacking sites in its PBP. We thought of three possible catalytic mechanisms for the step-

wise hydrolysis of (d)NTPs to (d)NMPs and orthophosphates (Fig. 8). [We selected GTP as a substrate to propose the mechanism because GDP is the preferred substrate of YmfB (Xu *et al.*, 2006).] The first mechanism requires two different substrate phosphate-attacking sites. In the two-attacking-sites mechanism, the γ -phosphate of GTP would be next to the β -phosphate of GDP in the YmfB–GDP complex. The γ - and β -phosphates would be attacked in two different positions in a stepwise manner (Fig. 8*a*). The second mechanism acts with one attacking site. However, to carry out two consecutive hydrolysis reactions, the first hydrolysis product, GDP, must be shifted into the attacking site for the second hydrolysis reaction (Fig. 8*b*). It is unlikely that YmfB recognizes the base and the ribose of the nucleotides in two different ways within the same binding surface as GDP moves into the attacking site. In addition, the results of our enzyme-kinetic assays with site-directed mutants confirmed that YmfB recognizes GDP specifically. The third mechanism, also with one attacking site, proposes specific substrate recognition of the base and the ribose, and only the binding of the substrate phosphates is different between GTP and GDP (Fig. 8*c*). The one-attacking-site mechanism is possible when the γ -phosphate of GTP is positioned at the same position as the β -phosphate of GDP, aided by the flexibility of the substrate phosphates. After hydrolysis of the γ -phosphate of GTP, the β -phosphate of the product GDP would move into the previous γ -phosphate position of GTP for additional hydrolysis. In this mechanism the stepwise hydrolysis of substrate phosphates could be accomplished using only one reaction site.

To elucidate the mechanism, we mutated the residues which might recognize or interact directly with the substrates GTP or GDP and studied the kinetic properties of each mutant. As for all other Nudix hydrolases, mutations of metal-coordinating residues abolished the YmfB enzymatic activity completely. However, mutation of no other active-site residue had a major effect on catalysis, *i.e.* it appears that YmfB has no catalytic base to deprotonate the attacking water molecule. Only two mutants, E54Q and D98N, showed a different effect on their relative catalytic efficiencies for GTP and GDP, but the differences were not large: the relative activities for GTP were approximately twofold lower than those for GDP. This suggested that both residues are more involved in the hydrolysis of GTP than GDP. Both residues are located close to each other and are also just outside of the two metal-binding sites and the putative β -phosphate binding site (Fig. 9).

Because the activity of the site-directed mutants did not provide decisive evidence for a key catalytic base among all of the available nearby residues, we evaluated the possibility of hydrolysis without a catalytic base. We focused on the hydrolysis mechanism of GDP, the highest activity substrate (Xu *et al.*, 2006), and carried out thermodynamic integration calculations to determine whether the species bound to the two metal ions might be a hydroxide ion, which could directly attack the β -phosphate of GDP. The calculations show that a hydroxide ion bound between two metal ions is more stable than a water molecule by 14.5 kcal mol⁻¹ under standard (1 M) conditions (2.4 kcal mol⁻¹ in water). This energy

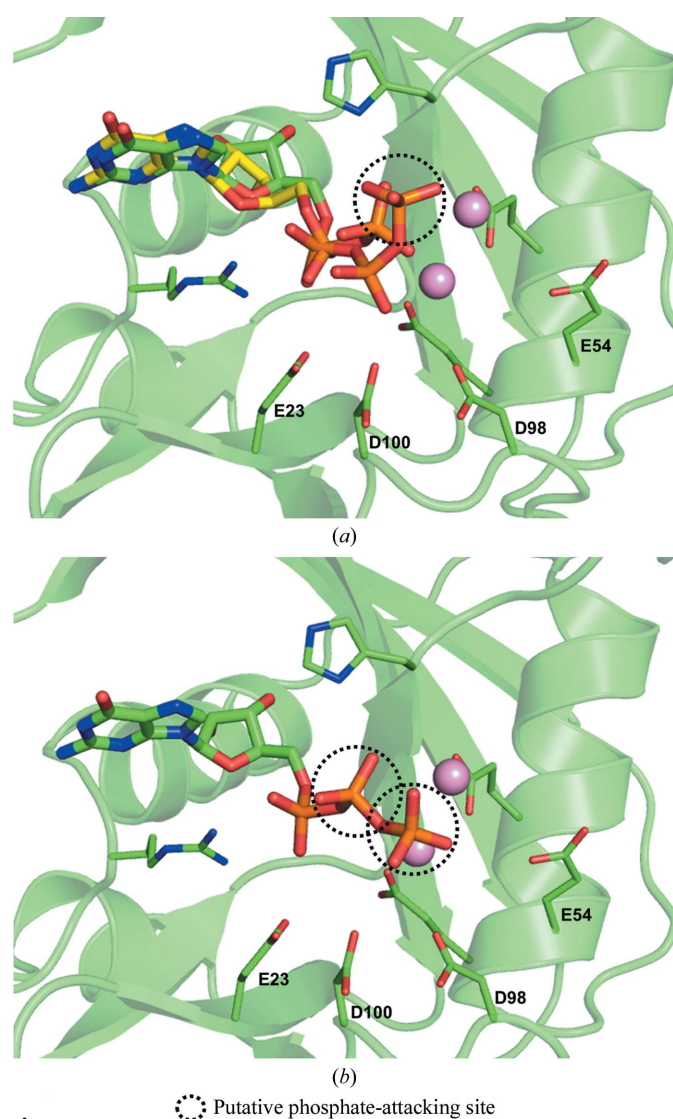


Figure 9 Molecular-docked models of YmfB recognizing GTP and two Mn²⁺ ions. (a) and (b) are shown in two possible GTP-bound conformations. The superimposed models of bound GDP (green C atoms) and GTP (yellow C atoms) are represented. The putative phosphate-attacking sites are represented as dotted circles. Bound GTP and the two Mn²⁺ ions are represented as sticks and spheres, respectively.

corresponds to a pK_a of the metal-bound water of 5.2. At neutral pH, it is 45 times more probable to find a hydroxide ion bound to the metal ions than a water molecule. At higher pH, the recruitment of a hydroxide ion into the active site would be even easier. The higher catalytic activity of YmfB at higher pH also supports the proposed direct binding of a hydroxyl ion to the two metal ions (Supplementary Fig. S2).

Interestingly, DR1025, which was found to have a similar structure to YmfB by the *DALI* server, has both the atypical hydrolysis activity and an unusually extensive negatively charged surface in the PBP (Ranatunga *et al.*, 2004; Fig. 7). In YmfB, the Glu54 and Asp98 residues are located just outside the two metal-binding sites and constitute the extensive negatively charged surface in PBP. The extensive negative charge of Glu54 and Asp98 at the outside of the metal-binding sites could prohibit binding of the γ -phosphate of GTP (Fig. 9*b*) and help the GTP phosphates to bind in the bent conformation required for the one-attacking-site mechanism (Fig. 9*a*). A hydroxyl ion could bind between the divalent metal ions at the active site directly, the γ -phosphate of GTP could be attacked by a hydroxyl ion and the resulting GDP product could be hydrolyzed again by a slight shift of the β -phosphate to the attacking position next to the two metal ions. Accordingly, two hydroxyl ions could attack the γ -phosphate of GTP and β -phosphate of GDP sequentially. GMP and two orthophosphates would be released as products.

In this paper, the structures of YmfB alone and in complex with two manganese metal ions and three sulfate anions were determined. From the results of mass spectrometry, molecular docking, structural comparisons, enzyme-kinetic measurements of site-directed mutants and thermodynamic integration calculations, we propose GDP- and GTP-binding models and a mechanism for the atypical hydrolysis by YmfB. In this mechanism, binding to the metal ions lowers the pK_a of the reactive water to 5.2 and the resulting bound hydroxyl can carry out nucleophilic attack without the help of a catalytic base from the protein.

We are grateful to Dr L. Mario Amzel for discussion and comment on this paper. We are grateful to Dr K. J. Kim and Dr Y. G. Kim for their assistance at beamlines 4A and 6C of the Pohang Light Source (PLS), Republic of Korea and to staff members at beamline 17A of the Photon Factory (KEK), Japan. This work was supported by WTU Research Grants of Konkuk University.

References

- Abagyan, R., Totrov, M. & Kuznetsov, D. (1994). *J. Comput. Chem.* **15**, 488–506.
- Abdelghany, H. M., Bailey, S., Blackburn, G. M., Rafferty, J. B. & McLennan, A. G. (2003). *J. Biol. Chem.* **278**, 4435–4439.
- Abdelghany, H. M., Gasmi, L., Cartwright, J. L., Bailey, S., Rafferty, J. B. & McLennan, A. G. (2001). *Biochim. Biophys. Acta*, **1550**, 27–36.
- Abeygunawardana, C., Weber, D. J., Gittis, A. G., Frick, D. N., Lin, J., Miller, A. F., Bessman, M. J. & Mildvan, A. S. (1995). *Biochemistry*, **34**, 14997–15005.
- Ames, B. N. & Dubin, D. T. (1960). *J. Biol. Chem.* **235**, 769–775.
- Bailey, S., Sedelnikova, S. E., Blackburn, G. M., Abdelghany, H. M., Baker, P. J., McLennan, A. G. & Rafferty, J. B. (2002). *Structure*, **10**, 589–600.
- Bessman, M. J., Frick, D. N. & O'Handley, S. F. (1996). *J. Biol. Chem.* **271**, 25059–25062.
- Bhatnagar, S. K. & Bessman, M. J. (1988). *J. Biol. Chem.* **263**, 8953–8957.
- Bhatnagar, S. K., Bullions, L. C. & Bessman, M. J. (1991). *J. Biol. Chem.* **266**, 9050–9054.
- Bradbrook, G. M., Gleichmann, T., Harrop, S. J., Habash, J., Rafferty, J., Kalb (Gilboa), J., Yariv, J., Hillier, I. H. & Helliwell, J. R. (1998). *J. Chem. Soc. Faraday Trans.* **94**, 1603–1611.
- Case, D. A. *et al.* (2008). *AMBER 10*. University of California, San Francisco, USA.
- Conyers, G. B., Wu, G., Bessman, M. J. & Mildvan, A. S. (2000). *Biochemistry*, **39**, 2347–2354.
- Emsley, P., Lohkamp, B., Scott, W. G. & Cowtan, K. (2010). *Acta Cryst.* **D66**, 486–501.
- Essmann, U., Perera, L., Berkowitz, M. L., Darden, T., Lee, H. & Pedersen, L. G. (1995). *J. Chem. Phys.* **103**, 8577.
- Frick, D. N., Weber, D. J., Gillespie, J. R., Bessman, M. J. & Mildvan, A. S. (1994). *J. Biol. Chem.* **269**, 1794–1803.
- Gabelli, S. B., Bianchet, M. A., Bessman, M. J. & Amzel, L. M. (2001). *Nature Struct. Mol. Biol.* **8**, 467–472.
- Gabelli, S. B., Bianchet, M. A., Ohnishi, Y., Ichikawa, Y., Bessman, M. J. & Amzel, L. M. (2002). *Biochemistry*, **41**, 9279–9285.
- Harris, T. K., Wu, G., Massiah, M. A. & Mildvan, A. S. (2000). *Biochemistry*, **39**, 1655–1674.
- Holm, L., Kääriäinen, S., Wilton, C. & Plewczynski, D. (2006). *Curr. Protoc. Bioinformatics*, Unit 5.5. doi:10.1002/0471250953.bi0505s14.
- Hong, M.-K., Kim, J.-K., Ahn, Y.-J. & Kang, L.-W. (2009). *Protein Pept. Lett.* **16**, 101–104.
- Jorgensen, W. L., Chandrasekhar, J., Madura, J. D., Impey, R. W. & Klein, M. L. (1983). *J. Chem. Phys.* **79**, 926.
- Kang, L.-W., Gabelli, S. B., Cunningham, J. E., O'Handley, S. F. & Amzel, L. M. (2003). *Structure*, **11**, 1015–1023.
- Kirschner, K. N., Yongye, A. B., Tschampel, S. M., González-Outeiriño, J., Daniels, C. R., Foley, B. L. & Woods, R. J. (2008). *J. Comput. Chem.* **29**, 622–655.
- Laskowski, R. A., MacArthur, M. W., Moss, D. S. & Thornton, J. M. (1993). *J. Appl. Cryst.* **26**, 283–291.
- Lawhorn, B. G., Gerdes, S. Y. & Begley, T. P. (2004). *J. Biol. Chem.* **279**, 43555–43559.
- Legler, P. M., Lee, H. C., Peisach, J. & Mildvan, A. S. (2002). *Biochemistry*, **41**, 4655–4668.
- Leslie, N. R., McLennan, A. G. & Safrany, S. T. (2002). *BMC Biochem.* **3**, 20.
- Lin, J., Abeygunawardana, C., Frick, D. N., Bessman, M. J. & Mildvan, A. S. (1997). *Biochemistry*, **36**, 1199–1211.
- Lin, S., Gasmi, L., Xie, Y., Ying, K., Gu, S., Wang, Z., Jin, H., Chao, Y., Wu, C., Zhou, Z., Tang, R., Mao, Y. & McLennan, A. G. (2002). *Biochim. Biophys. Acta*, **1594**, 127–135.
- Marshall, W. L. & Franck, E. U. (1981). *J. Phys. Chem. Ref. Data*, **10**, 295.
- McLennan, A. G. (2006). *Cell. Mol. Life Sci.* **63**, 123–143.
- Méjean, V., Salles, C., Bullions, L. C., Bessman, M. J. & Claverys, J. P. (1994). *Mol. Microbiol.* **11**, 323–330.
- Mildvan, A. S., Xia, Z., Azurmendi, H. F., Saraswat, V., Legler, P. M., Massiah, M. A., Gabelli, S. B., Bianchet, M. A., Kang, L.-W. & Amzel, L. M. (2005). *Arch. Biochem. Biophys.* **433**, 129–143.
- Murzin, A. G., Brenner, S. E., Hubbard, T. & Chothia, C. (1995). *J. Mol. Biol.* **247**, 536–540.
- Pang, Y.-P. (2001). *Proteins*, **45**, 183–189.
- Ranatunga, W., Hill, E. E., Mooster, J. L., Holbrook, E. L., Schulze-Gahmen, U., Xu, W., Bessman, M. J., Brenner, S. E. & Holbrook, S. R. (2004). *J. Mol. Biol.* **339**, 103–116.

- Simonson, T., Carlsson, J. & Case, D. A. (2004). *J. Am. Chem. Soc.* **126**, 4167–4180.
- Tanaka, M., Girard, G., Davis, R., Peuto, A. & Bignell, N. (2001). *Metrologia* **38**, 301.
- Wang, Z., Jiao, X., Carr-Schmid, A. & Kiledjian, M. (2002). *Proc. Natl Acad. Sci. USA*, **99**, 12663–12668.
- Warshel, A., Sussman, F. & King, G. (1986). *Biochemistry*, **25**, 8368–8372.
- Winn, M. D. *et al.* (2011). *Acta Cryst.* **D67**, 235–242.
- Xu, W., Dunn, C. A. & Bessman, M. J. (2000). *Biochem. Biophys. Res. Commun.* **273**, 753–758.
- Xu, W., Dunn, C. A., O’Handley, S. F., Smith, D. L. & Bessman, M. J. (2006). *J. Biol. Chem.* **281**, 22794–22798.
- Xu, W., Shen, J., Dunn, C. A. & Bessman, M. J. (2003). *FASEB J.* **17**, A574.
- Xu, W., Shen, J., Dunn, C. A., Desai, S. & Bessman, M. J. (2001). *Mol. Microbiol.* **39**, 286–290.
- Yagi, T., Baroja-Fernández, E., Yamamoto, R., Muñoz, F. J., Akazawa, T., Hong, K. S. & Pozueta-Romero, J. (2003). *Biochem. J.* **370**, 409–415.
- Yanofsky, C., Cox, E. C. & Horn, V. (1966). *Proc. Natl Acad. Sci. USA*, **55**, 274–281.